This is the accepted manuscript made available via CHORUS. The article has been published as:

Incommensurate Spin-Density Wave Order in Electron-Doped BaFe_{2}As_{2} Superconductors

D. K. Pratt, M. G. Kim, A. Kreyssig, Y. B. Lee, G. S. Tucker, A. Thaler, W. Tian, J. L. Zarestky, S. L. Bud'ko, P. C. Canfield, B. N. Harmon, A. I. Goldman, and R. J. McQueeney

Phys. Rev. Lett. **106**, 257001 — Published 20 June 2011

DOI: 10.1103/PhysRevLett.106.257001

Incommensurate spin-density wave order in electron-doped $BaFe_2As_2$ superconductors

D. K. Pratt, M. G. Kim, A. Kreyssig, Y. B. Lee, G. S. Tucker, A. Thaler, W. Tian,
J. L. Zarestky, S. L. Bud'ko, P. C. Canfield, B. N. Harmon, A. I. Goldman, and R. J. McQueeney

Ames Laboratory, US DOE and Iowa State University, Ames, IA 50011, USA

Neutron diffraction studies of $Ba(Fe_{1-x}Co_x)_2As_2$ reveal that commensurate antiferromagnetic order gives way to incommensurate magnetic order for Co compositions between $0.056 < x < 0.06$. The incommensurability has the form of a small transverse splitting $(0, \pm\epsilon, 0)$ from the commensurate antiferromagnetic propagation vector $\mathbf{Q}_{\rm AFM} = (1, 0, 1)$ (in orthorhombic notation) where $\boldsymbol{\epsilon} \approx 0.03 - 0.03$ and is composition dependent. The results are consistent with the formation of a spin-density wave driven by Fermi surface nesting of electron and hole pockets and confirm the itinerant nature of magnetism in the iron arsenide superconductors.

PACS numbers: 74.70.Xa,75.25.-j, 75.30.Fv, 75.30.Kz

Unconventional superconductivity is often associated with the pairing of electrons via spin fluctuations that appear close to a magnetic ordering instability. In this respect, the nature and origin of the magnetic instability itself is an important ingredient of any theory of superconductivity. In the iron arsenide compounds, the magnetism has been discussed from two limits; an itinerant and a local moment limit. The parent AFe_2As_2-based superconductors (A = Ca, Sr, Ba) are antiferromagnetic (AFM) metals, which suggests that an itinerant description is an appropriate starting point. AFM order is observed with a commensurate magnetic propagation vector $\mathbf{Q}_{\rm AFM} = (1, 0, 1)$ (expressed in orthorhombic notation) by neutron and x-ray resonant magnetic diffraction.[1–9] The small ordered magnetic moments measured ($< 1\mu_B$) also favor an itinerant description. In principle, the propagation vector of the AFM order itself, $\mathbf{Q}_{\rm AFM}$, should further strengthen the case for itinerant magnetism, as both band structure calculations [10, 11] and angle-resolved photoemission data [12–14] display Fermi surface nesting between electron and hole pockets with a nesting vector close to $\mathbf{Q}_{\rm AFM}$. Here we define an itinerant spin-density wave (SDW) as magnetic order resulting from an instability due to such Fermi surface nesting, with the best known example being the incommensurate (IC) SDW order observed in Cr metal.[15] However, the commensurate (C) AFM order observed at $\mathbf{Q}_{\rm AFM}$ can also be described within a local moment picture that may become relevant in the presence of moderately large electronic correlations and can be quantified, for example, in terms of the $J_1 - J_2$ Heisenberg model where $J_2 > 2J_1$.[16]

Detailed band structure calculations of the magnetic susceptibility in the iron arsenides predict that the Fermi surface nesting condition can result in either C-SDW order at $\mathbf{Q}_{\rm AFM}$, or IC-SDW order with a propagation vector $\boldsymbol{\tau} = \mathbf{Q}_{\rm AFM} + \boldsymbol{\epsilon}$ where $\boldsymbol{\epsilon}$ is a small incommesurability.[17, 18] Although the observation of IC magnetic order would clearly favor an itinerant SDW description of the AFe_2As_2 system, detailed magnetic diffraction studies have observed only C-AFM order with a propagation vector $\mathbf{Q}_{\rm AFM}$ in several AFe_2As_2 systems including the parent compounds [1–3] and doped compounds: $Ba(Fe_{1-x}Co_x)_2As_2$,[4–6] $Ba(Fe_{1-x}Ni_x)_2As_2$,[7] $Ba(Fe_{1-x}Rh_x)_2As_2$,[8] $Ba(Fe_{1-x}Ru_x)_2As_2$,[9] $Ba_{1-x}K_xFe_2As_2$.[19] Incommensurability has been claimed in $Ba(Fe_{1-x}Co_x)_2As_2$ by local probes such as ^{75}As nuclear magnetic resonance [20], ^{57}Fe Mössbauer [21], and muon spin resonance [22] measurements. However, detailed measurements of the AFM ordering by both neutron and high resolution x-ray resonant magnetic diffraction have found no incommensurability in $Ba(Fe_{1-x}Co_x)_2As_2$ up to $x = 0.047$.[6]

In this Letter, neutron diffraction data demonstrate that IC magnetic order does indeed develop near optimally doped compositions of $Ba(Fe_{1-x}Co_x)_2As_2$ with $x \geq 0.056$, just before long-range magnetic ordering is completely suppressed at $x \approx 0.06$. The IC propagation vector $\boldsymbol{\tau} = \mathbf{Q}_{\rm AFM} + (0, \epsilon, 0)$ corresponds to a transverse splitting ($\epsilon \approx 0.02 - 0.03$) whose value depends on composition. The direction and magnitude of the observed IC splitting is consistent with calculations of the generalized susceptibility determined by density functional theory, allowing us to conclude that static magnetism and the spin fluctuations for superconducting compositions are tied to an itinerant SDW instability.

Single-crystals of $Ba(Fe_{1-x}Co_x)_2As_2$ were prepared using a solution growth technique described elsewhere [23] with the following compositions (and masses); $x = 0.054$ (124 mg), 0.056 (248 mg), 0.057 (73 mg), 0.059 (136 mg), and 0.062 (106 mg). The sample compositions were determined through a series of characterization measurements including resistivity, magnetization, and wavelength dispersive spectroscopy (WDS).[23] All samples are orthorhombic below the tetragonal-orthorhombic transition temperature (T_S) and the data are discussed in terms of the orthorhombic indexing $\mathbf{Q} = (\frac{2\pi H}{a}\ \frac{2\pi K}{b}\ \frac{2\pi L}{c})$

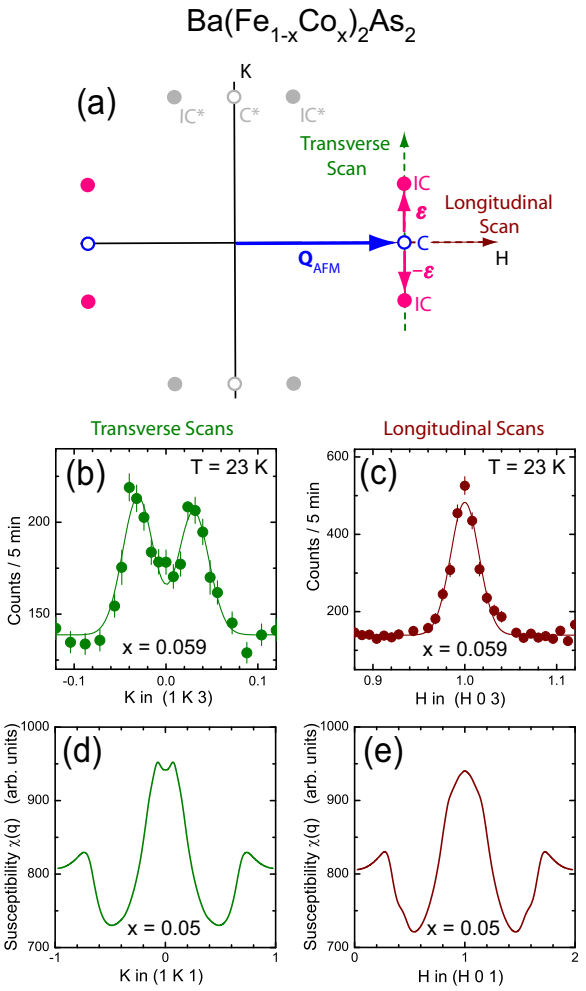

FIG. 1: (a) Reciprocal space plane with L = *odd* indicating commensurate (C, empty circles) and incommensurate (IC, filled circles) magnetic Bragg peak positions at $\mathbf{Q}_{\rm AFM}$ = (1, 0, L = *odd*) and $\boldsymbol{\tau}$ = (1, $\pm\epsilon$, L = *odd*), respectively, in orthorhombic notation. The size of the incommensurability parameter is exaggerated for clarity. Shaded points labeled C* and IC* show the location of magnetic Bragg peaks that are present due to orthorhombic twinning. Dashed arrows illustrate the direction of longitudinal [H, 0, 0] and transverse [0, K, 0] neutron diffraction scans. Raw (b) transverse and (c) longitudinal scans for $Ba(Fe_{0.941}Co_{0.059})_2As_2$ at T = 23 K $\approx$ T_c. The lines are Gaussian fits to the data. *Ab initio* calculations of the generalized susceptibility in the (d) transverse and (e) longitudinal directions through $\mathbf{Q}_{\rm AFM}$.

where $a \approx b \approx 5.6\mathring{A}$ and $c \approx 13\mathring{A}$. The characteristic phase transition temperatures T_S, T_N (antiferromagnetic ordering temperature), and T_c (superconducting transition temperature) were determined using similar procedures outlined previously.[5, 24] T_N was determined by the break in slope of the integrated neutron intensity (order parameter) at $\mathbf{Q}_{\rm AFM}$ separating Bragg scattering from a "tail" of critical scattering or magnetic short-range order that can persist above T_N. This method can lead to a small uncertainty in the true value of T_N for the weak magnetic signals encountered in this study. However, all reported transition temperatures (T_S, T_N, and T_c) are consistent with our current understanding of the phase diagram of $Ba(Fe_{1-x}Co_x)_2As_2$.[25] The sharpness of the superconducting transition, predictable evolution of T_S and T_N with relatively small changes in composition, and uniformity of the WDS signal at multiple locations on the crystals confirm good chemical homogeneity with compositional spread $\frac{\delta x}{x} < 5\%$.[23]

Neutron diffraction measurements were performed at Oak Ridge National Laboratory using the High Flux Isotope Reactor's HB1A triple axis spectrometer using a horizontal collimation 48'-48'-40'-68' and E_i = 14.7 meV. All samples have resolution-limited mosaic full-widths of < 0.4 degrees and were mounted in a closed-cycle refrigerator. Samples were studied in the vicinity of $\mathbf{Q}_{\rm AFM}$ = (1, 0, 1) and (1, 0, 3) in two scattering planes; in the (H, 0, L) plane, allowing the search for IC splitting along the orthorhombic **a** axis ([H, 0, 0] is referred to as the longitudinal direction), and in the (ζ, K, 3ζ) or (ζ, K, ζ) planes, allowing the search for incommensurability along the **b** axis ([0, K, 0], transverse direction). [See Fig. 1(a)]

Typical transverse [0, K, 0] and longitudinal [H, 0, 0] neutron diffraction scans are shown in Figs. 1(b) and (c) for the x = 0.059 sample at $T \approx T_c < T_N$, where magnetic Bragg intensity is a maximum. The observation of a pair of Bragg peaks located symmetrically at positions (0, $\pm\epsilon$, 0) around $\mathbf{Q}_{\rm AFM}$ in the transverse scan clearly indicates IC magnetic order for this composition. No longitudinal splitting is observed, therefore IC magnetic order is present with propagation vector $\boldsymbol{\tau}$ = (1, ϵ, 1) = $\mathbf{Q}_{\rm AFM}$ + (0, ϵ, 0), as illustrated in Fig. 1(a).

We now turn to *ab initio* density functional calculations of the magnetic susceptibility in order to show that the observed IC-AFM order can be understood as a SDW driven by Fermi surface nesting. Previous calculations show maxima in the generalized spin susceptibility away from $\mathbf{Q}_{\rm AFM}$ in doped AFe_2As_2 compounds and therefore point to a tendency for IC-SDW order.[17, 18] To gain insight into potential incommensurability at doping levels where we observe static IC-AFM order, we performed calculations of the generalized bare susceptibility employing the full-potential linearized augmented plane wave (FPLAPW) method,[26] with a local density functional.[27] We used $R_{\rm MT}K_{\rm max} = 8.0$ and $R_{\rm MT}$ = 2.4, 2.2 and 2.2 for Ba, Fe and As, respectively. To obtain self-consistency we chose 550 **k**-points in the irreducible Brillouin zone and used 0.01 mRy/cell as the total energy convergence criteria. The virtual crystal approximation was used to consider Co-doping effects and the whole reciprocal unit cell is divided into 80 × 80 × 80 parallelepipeds, corresponding to 34061 irreducible **k**-points. Our calculations of the generalized susceptibility for electron doping with x = 0.05 show splitting in the transverse direction and a single peak in the longitudinal direction in Figs. 1(d) and 1(e), respectively, consistent with other

doping dependent calculations.[17, 18] The *ab initio* calculations, therefore, show a tendency for IC-SDW order with propagation vector $\boldsymbol{\tau} \approx \mathbf{Q}_{\rm AFM} + (0, \epsilon, 0)$ in agreement with experimental observations.

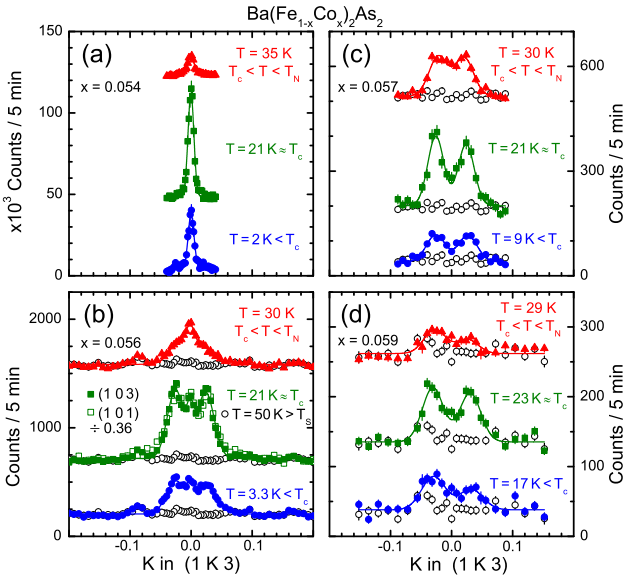

FIG. 2: Transverse neutron diffraction scans at temperatures $T < T_c$ (blue circles), $T \approx T_c$ (green squares), $T_c < T < T_N$ (red triangles), and $T > T_S$ (empty circles) for $Ba(Fe_{1-x}Co_x)_2As_2$ with x = (a) 0.054, (b) 0.056, (c) 0.057, and (d) 0.059. Scans with $T > T_S$ are an estimate of the background. All scans are performed through the (1, 0, 3) position except the empty green squares in (b), which are measured through (1, 0, 1) and with the intensity divided by a factor of 0.36. The lines are Gaussian fits to the data.

Figure 2 shows the transverse [0, K, 0] scans through (1, 0, 3) for other compositions and temperatures. The scans performed at temperatures above T_S serve as an estimate of the background. The propagation vector, peak widths, and integrated intensities were determined by Gaussian fits to the scans shown in Fig. 2. The transverse [0, K, 0] scans show only a single resolution-limited peak for the $x = 0.054$ sample and, combined with x-ray resonant magnetic diffraction results from M. G. Kim *et al.* [6], establish stripe-type C-AFM order at $\mathbf{Q}_{\rm AFM}$ for all Co compositions below approximately 0.054. Broad peaks split in the transverse direction are observed in [0, K, 0] scans for $x = 0.056$, 0.057, and 0.059, clearly establishing the transition to an IC magnetic phase with propagation vector $\boldsymbol{\tau}$. For the $x = 0.056$ sample, both C and IC peaks are observed, suggesting that the transition is first-order in its dependence on Co concentration with the the phase boundary close to $x = 0.056$. The coexistence of C and IC phases could arise from a small spread in the Co concentration across the sample, as noted above. Figure 2(b) shows that the lineshapes at (1, 0, 3) and (1, 0, 1) positions are equivalent with an integrated intensity ratio of 0.36(9), close to that expected for collinear C-AFM order with the magnetic moment pointing along the **a** axis. Therefore, the IC-AFM structure is most likely also collinear, and not helical or cycloidal. No signatures of higher harmonics have been observed, indicating a sinusoidal modulation of the moment size along the **b** direction.

We now discuss the temperature dependence of transverse scans shown in Fig. 2. For $x = 0.054$ [Fig. 2(a)], the suppression of the integrated intensity (magnetic order parameter) below T_c indicates the competition of C-AFM with superconductivity, as reported previously.[5, 24, 28] The magnetic intensity in Figs. 2(b) - (d) show a similar suppression below T_c implying that the IC-AFM state also competes with superconductivity.

Figure 3(a) shows the experimental phase diagram of $Ba(Fe_{1-x}Co_x)_2As_2$ delineating regions of magnetic order, superconductivity, and structural phases as based on previous studies. [9–11, 23–25]. This work, summarized in Figs. 3(b) - (d), has allowed us to outline regions of C and IC magnetic order in the phase diagram. Fig. 3(b) shows the evolution from C (at $x = 0.054$) to IC-AFM order (from $x = 0.056 - 0.059$) in transverse scans performed at $T \approx T_c$. The $x = 0.062$ sample has no detectable magnetic order. The composition dependence of both the integrated magnetic intensity and incommensurability is plotted in Fig. 3(c) at $T \approx T_c$, again highlighting that the transition to IC magnetic order occurs at $x \approx 0.056$ in the limit where the magnetic intensity (moment size) is very small. The incommensurability grows slightly at the higher compositions, reaching a value of 0.030(2) at $x = 0.059$. Figure 3(d) displays the temperature dependence of the integrated intensity of IC-AFM Bragg peaks for the $x = 0.056$ sample, which has the characteristic suppression in the superconducting state, as alluded to above. Figure 3(d) shows the incommensurability parameter, ϵ, of the $x = 0.056$ sample remains relatively constant below T_c.

The magnetic phase diagram shown in Fig. 3(a) contains a first-order C-to-IC transition with electron doping in $Ba(Fe_{1-x}Co_x)_2As_2$ that bears a strong similarity to the alloys of the canonical SDW system, Cr. Pure Cr orders into an IC-SDW state that is driven by nesting between electron and hole Fermi surfaces whose areas are slightly mismatched.[15] Electron doping of Cr (in this case by alloying with Mn [29] or Ru [30]) equalizes the Fermi surface areas and results in a first-order transition to C-SDW order. This simple picture considers only the Fermi surface topology and the free energy of competing C and IC-SDW states and has led to a detailed theoretical understanding of the magnetic phase diagram of Cr alloys.[31]

The development of C or IC-SDW order has also been studied in the iron arsenides using an effective two-dimensional, two-band Ginzburg-Landau approach.[10, 32] In a spirit similar to Cr, IC-SDW order is favored when nesting occurs between electron and hole pock-

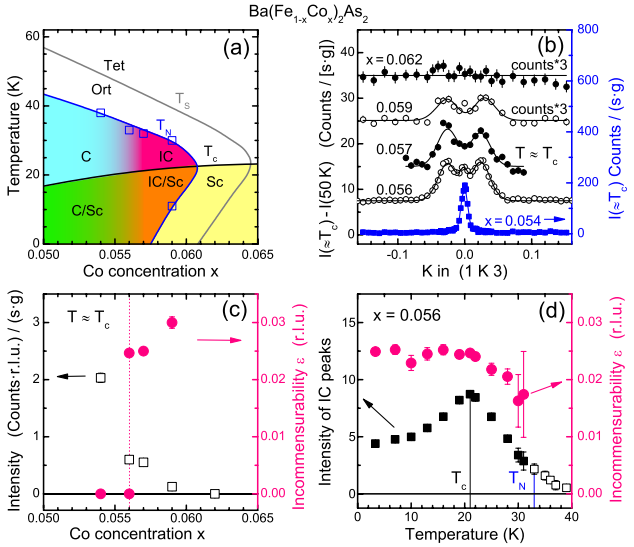

FIG. 3: (a) Experimental phase diagram for $Ba(Fe_{1-x}Co_x)_2As_2$ showing commensurate (C) and incommensurate (IC) antiferromagnetic order below T_N. Tetragonal (Tet) and orthorhombic (Ort) phases are separated by the phase line at T_S. Superconductivity (Sc) appears below T_c and can coexist with both commensurate (C/Sc) and incommensurate (IC/Sc) magnetic order. Open squares represent the magnetic phase transition temperatures determined in this study. (b) Background subtracted transverse neutron diffraction scans at $T \approx T_c$. Scans are offset vertically and scaled (where noted) for clarity. Integrated intensity (squares) and incommensurability parameter ϵ (circles) (c) as a function of Co concentration at $T \approx T_c$ and (d) as a function of temperature for $x = 0.056$. Open squares in (d) represent the total magnetic intensity where C and IC peaks cannot be separated.

ets having circular cross-sections of unequal area at the Fermi level. The introduction of more realistic elliptical electron pockets favor C-SDW order as long as the electron and hole pocket areas are not too strongly mismatched, as is the case for the parent AFe_2As_2 compounds. However, even with elliptical electron pockets, doping detunes the two pockets and eventually results in a mismatch that favors IC-SDW order. This analysis suggests that Fermi surface nesting is a crucial factor in stabilizing both C and IC phases in the magnetic phase diagram of the AFe_2As_2 compounds.

Unlike Cr, the doped iron arsenides are superconductors, and both C and IC-SDW order are observed to coexist with superconductivity. Ginzburg-Landau models [10, 32] indicate that the competition and coexistence of superconductivity with either C or IC-SDW order is much more likely with an unconventional s^{+-} pairing symmetry. Thus, a simple two-band approach appears to capture many of the essential features of the phase diagram of the AFe_2As_2 arsenides in terms of Fermi surface nesting, C and IC-SDW order, and unconventional s^{+-} superconductivity. The resulting theoretical phase diagram in Ref. [32] bears close resemblance to the experimental diagram in Fig. 3(a).

We acknowledge valuable discussions with J. Schmalian, R. M. Fernandes, T. Brueckel, and R. Hermann. This work was supported by the Division of Materials Sciences and Engineering, Office of Basic Energy Sciences, U.S. Department of Energy (U.S. DOE). Ames Laboratory is operated for the U.S. DOE by Iowa State University under Contract No. DE-AC02-07CH11358. The work at the High Flux Isotope Reactor, Oak Ridge National Laboratory (ORNL), was sponsored by the Scientific User Facilities Division, Office of Basic Energy Sciences, U.S. DOE. ORNL is operated by UT-Battelle, LLC for the U.S. DOE under Contract No. DE-AC05-00OR22725.

[1] A. I. Goldman et al., Phys. Rev. B **78**, 100506 (2008).
[2] J. Zhao et al., Phys. Rev. B **78**, 140504 (2008).
[3] Q. Huang et al., Phys. Rev. Lett. **101**, 257003 (2008).
[4] C. Lester et al., Phys. Rev. B **79**, 144523 (2009).
[5] R. M. Fernandes et al., Phys. Rev. B **81**, 140501 (2010).
[6] M. G. Kim et al., Phys. Rev. B **82**, 180412 (2010).
[7] M. Wang et al., Phys. Rev. B **81**, 174524 (2010).
[8] A. Kreyssig et al., Phys. Rev. B **81**, 134512 (2010).
[9] M. G. Kim et al., Phys. Rev. B **83**, 054514 (2011).
[10] A. B. Vorontsov et al., Phys. Rev. B **79**, 060508 (2009).
[11] V. Cvetkovic and Z. Tesanovic, Phys. Rev. B **80**, 024512 (2009).
[12] J. Fink et al., Phys. Rev. B **79**, 155118 (2009).
[13] P. Vilmercati et al., Phys. Rev. B **79**, 220503 (2009).
[14] C. Liu et al., Nat. Phys. **6**, 419423 (2010).
[15] E. Fawcett et al., Rev. Mod. Phys. **66**, 25 (1994).
[16] Q. Si and E. Abrahams, Phys. Rev. Lett. **101**, 076401 (2008).
[17] J. T. Park et al., Phys. Rev. B **82**, 134503 (2010).
[18] S. Graser et al., Phys. Rev. B **81**, 214503 (2010).
[19] H. Chen et al., Europhys. Lett. **85**, 17006 (2009).
[20] Y. Laplace et al., Phys. Rev. B **80**, 140501 (2009).
[21] P. Bonville et al., Europhys. Lett. **89**, 67008 (2010).
[22] P. Marsik et al., Phys. Rev. Lett. **105**, 057001 (2010).
[23] N. Ni et al., Phys. Rev. B **78**, 214515 (2008).
[24] D. K. Pratt et al., Phys. Rev. Lett. **103**, 087001 (2009).
[25] S. Nandi et al., Phys. Rev. Lett. **104**, 057006 (2010).
[26] P. Blaha et al., *WIEN2k, An Augmented Plan Wave + Local Orbitals Program for Calculation Crystal Properties* (TU Wien, Austria) (2001).
[27] J. P. Perdew and Y. Wang, Phys. Rev. B **45**, 13244 (1992).
[28] A. D. Christianson et al., Phys. Rev. Lett. **103**, 087002 (2009).
[29] B. J. Sternlieb et al., Phys. Rev. B **50**, 16438 (1994).
[30] R. S. Eccleston et al., Condens. Matter **8**, 7837 (1996).
[31] R. S. Fishman and S. H. Liu, Phys. Rev. B **48**, 3820 (1993).
[32] A. B. Vorontsov et al., Phys. Rev. B **81**, 174538 (2010).